# Creation of an atlas of filter positions for fluence field modulated CT

Timothy P. Szczykutowicz[a)]
*Departments of Radiology and Medical Physics, University of Wisconsin-Madison, 1111 Highland Avenue, Madison, Wisconsin 53705*

James Hermus
*Department of Biomedical Engineering, University of Wisconsin-Madison, 1550 Engineering Drive, Madison, Wisconsin 53706*

(Received 10 September 2014; revised 9 February 2015; accepted for publication 24 February 2015; published 19 March 2015)

**Purpose:** Fluence field modulated CT (FFMCT) and volume of interest (VOI) CT imaging applications require adjustment of the profile of the x-ray fluence incident on a patient as a function of view angle. Since current FFMCT prototypes can theoretically take on an infinite number of configurations, measuring a calibration data set for all possible positions would not be feasible. The present work details a methodology for calculating an atlas of configurations that will span all likely body regions, patient sizes, patient positioning, and imaging modes. The hypothesis is that there exists a finite number of unique modulator configurations that effectively span the infinite number of possible fluence profiles with minimal loss in performance.
**Methods:** CT images of a head, shoulder, thorax, abdominal, wrist, and leg anatomical slices were dilated and contracted to model small, medium, and large sized patients. Additionally, the images were positioned from iso-center by three different amounts. The modulator configurations required to compensate for each image were computed assuming a FFMCT prototype, digital beam attenuator, (DBA), was set to equalize the detector exposure. Each atlas configuration should be different from the other atlas configurations. The degree of difference was quantified using the sum of the absolute differences in filter thickness between configurations. Using this metric, a set of unique wedge configurations for which no two configurations have a metric value smaller than some threshold can be constructed. Differences in the total number of incident photons between the unconstrained filters and the atlas were studied as a function of the number of atlas positions for each anatomical site and size/off-centering combination.
**Results:** By varying the threshold used in creating the atlas, it was found that roughly 322 atlas positions provided an incident number of photons within 20% of using 19 440 unique filters (the number of atlas entries ranged from 7213 to 1). Additionally, for VOI applications implemented with a single VOI region, the number of required filter configurations was expressed in a simple closed form solution.
**Conclusions:** The methodology proposed in this work will enable DBA-FFMCT and DBA-VOI imaging in the clinic without the need for patient specific air-scans to be performed. In addition, the methodology proposed here is directly applicable to other modulator designs such as piecewise linear, TomoTherapy multi leaf collimators, 2D fluid arrays, and inverse geometry CT.  [http://dx.doi.org/10.1118/1.4915123]

Key words: dose modulation, fluence field modulation, dynamic bowtie

## 1. INTRODUCTION

The use of different kV, tube current, and bowtie filter sizes on today's state-of-the-art CBCT and CT modalities allows for a modulation of the fluence incident on patients. However, on many commercially available CBCT and CT systems, one is not free to choose any combination of kV, mA, and bowtie filter. Often only several kV stations are available, the mA is often restricted due to tube heating constraints, and at most three different sized bowtie filters are available. While some of these limits are due to engineering constraints, some are mandatory to keep the amount of system calibration logistically feasible. The need for system calibration in CBCT and CT stems from the requirement to obtain projection data for image reconstruction. In order to create line integral projection data from transmitted signal intensity measurements, the fluence incident on the patient must be known. This is commonly referred to as collecting air-scan data as it is collected with no phantom object in place, hence the scan is taken entirely of air. This can be observed easily by considering Beer's law [$I = I_o \cdot \exp(-P)$]. If one desires the projection line integral $P$, one measures the signal recorded at the detector transmitted through the patient $I$, therefore the quantity incident on the patient $I_o$ must be known. In CBCT and CT imaging, $I_o$ varies as a function of fan angle due to the bowtie filter and the heel effect for a given mA and kV. As the mA and kV can change as a function of view angle due to dose modulation, calibration tables must

be made or models of the response of $I_o$ as a function of fan angle, kV, bowtie filter, and mA must be created.

The experimental implementation of fluence field modulated CT (FFMCT) developed in our previous work (Szczykutowicz and Mistretta[1–3]) used a scan specific method to calculate the air-scan data $I_o$. While this approach allowed for artifact free digital beam attenuator (DBA)-FFMCT and DBA-volume of interest (VOI) images to be created, it required an air-scan be performed using the same wedge configurations as were used to acquire the scan data when the phantom object was in the beam. In a clinical environment, this type of work flow would not be feasible, especially in an interventional CT or CBCT setting where the patient cannot easily be moved out of the scan field of view in the middle of a procedure.

Ray tracing through a DBA wedge pair is complicated as it requires modeling two right triangular prisms with a small air gap between them as shown in Fig. 1. We have successfully modeled them in a simulation setting, but our current experimental prototype does not have enough reproducibility to allow successful modeling of the wedges without artifacts due to slight differences between where the wedges are in the model and in reality. In addition, the beam hardening due to the wedges must be modeled accurately. This also can be modeled and empirically measured but is a time consuming process. These two issues have made creating a model for the attenuation from the DBA wedge difficult.

Simply measuring the air-scan value of each wedge pair independently at a variety of different thicknesses will not allow any arbitrary wedge configuration's air-scan to be obtained. This is due to x-rays traversing two sets of wedge pairs at the boundary between each wedge pair as shown in Fig. 1. Even if the filter array was made to be focused onto the x-ray source, due to the finite focal spot size, some rays would still traverse multiple filters as shown in Fig. 1. Therefore, in this paper, we take the same approach as that of today's CBCT and CT vendors; we assume physical measurements can be obtained for a range of operating points and that these operating points will span the range of clinically required configurations.

The methodology presented here is applicable to the FFMCT technology implemented by other research groups such as Hsieh and Pelc[4,5] and the simulation work being carried out by Bartolac and Jaffray.[6–8] In addition, the technique described in this work should have applications in VOI imaging.[9–14] Recently, the use of 2D and 1D arrays of attenuating fluids (liquids and gases) has been proposed[15,16] for FFMCT/VOI imaging and these approaches will likely face similar challenges as previously discussed. All of these techniques rely on imaging with a fluence field that changes from view to view or changes on a patient to patient basis.

## 2. MATERIALS AND METHODS

Table I lists the notations and abbreviations used in this paper. The guiding assumption made in this paper is that it is possible to use only a subset of all possible wedge configurations with a negligible effect in terms of dose and image quality. Wedge configuration refers to the arrangement of wedge pair thicknesses making up the DBA. When the wedge configuration for a given phantom at a given view angle is restricted to be selected from a set of precalibrated atlas wedge configurations, the difference in the corresponding incident fluence profile from the unconstrained wedge configuration and the atlas configuration should be minimal. The aim of this work is to detail a procedure for creating such an atlas and to provide a method for analyzing how many atlas entries are required to satisfy our assumption that an atlas can be used which will allow for a negligible loss in FFMCT performance. The criteria for what is considered a negligible loss are inherently subjective. In this paper, we propose a metric based on the change in the total number of photons incident on a patient which is a surrogate for patient dose. Future work by our group and other groups adopting this atlas methodology may choose to use criteria based on changes in detector dynamic range requirements[17] or changes in image noise nonuniformity to minimize the number of atlas entries.

### 2.A. Atlas calculation for DBA-FFMCT

The atlas should be capable of spanning all patient body regions, sizes, and positions [see Fig. 2(a)]. Different body

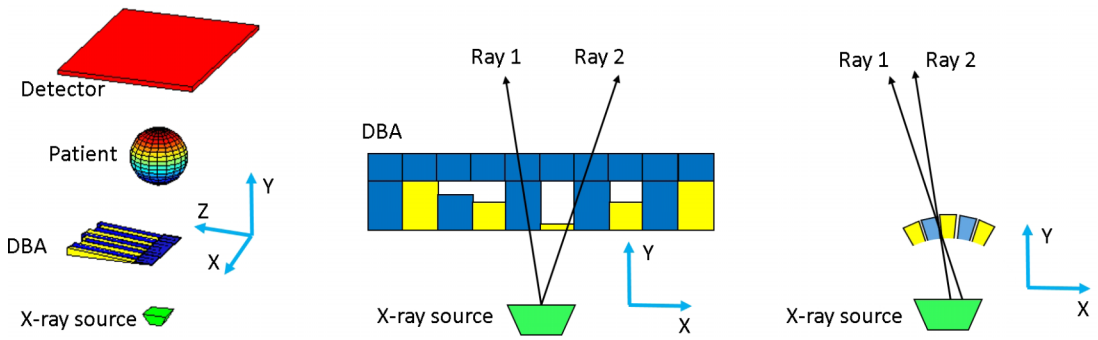


FIG. 1. (Left) Depiction of the DBA located in a typical CT acquisition geometry. (Middle) View depicting two x-ray paths. Ray 1 intersects a single pair of wedges. Ray 2 intersects three wedges. The air-scan value for Ray 2 will depend on the positioning of two different sets of wedge pairs. (Right) View depicting the case of a DBA made to be focused on the x-ray source. Due to the finite size of the focal spot, Ray 2 passes through two filters.

TABLE I. A summary of variables and abbreviations.

| Notation | Description |
|---|---|
| DBA | Digital beam attenuator |
| VOI | Volume of interest |
| *numConfigs* | Number of wedge pair configurations used to construct the atlas. |
| *n*DBA | Number of wedge pairs used to simulate a DBA (one wedge pair is required to modulate each wedgelet). |
| $i$ | Wedglet number, integer ranging from 1 to 10. |
| $v$ | Wedge configuration index, integer ranging from 1 to *numConfigs*. |
| $H(i,v)$ | Array of wedge configurations used to create the atlas. The values represent physical wedge thicknesses for each wedge pair. |
| tr | Threshold used to create an atlas. It represents the sum of thickness differences between two different wedge configurations. |
| $A(i,v)$ | Array of wedge configurations contained in the atlas. The values represent physical wedge thicknesses for each wedge pair. |
| $n_{\text{atlas}}$ | Index for different wedge pair configurations in the atlas. |

regions must be simulated to create an atlas due to the different tissues present in different body regions. For example, the shoulders represent a large change in attenuation in the lateral direction relative to the anterior–posterior direction while the thorax has a large change in attenuation over the anterior–posterior projections due to the lung fields and mediastinum. Different body sizes will require different thicknesses of DBA wedge configurations as well as engage more wedges further from the iso-ray than would be used for smaller patients. Different patient positions must be simulated because even for the same body region and patient size, the DBA configuration must change as the patient is moved away from iso-center.

The total number of view angles (*numConfigs*) used in the atlas computation is equal to the number of body regions times the number of body sizes times the number of offcentering positions times the number of view angles for each body region/body size/position sum to a total of 19 440 configurations. Each specific body size/region/position simulation used 360 view angles. A source to isocenter distance of 541 mm, 888 detector elements, a source to detector distance of 949 mm, and a fan angle of 54° were used. The number of DBA wedge pairs (*n*DBA) was ten and therefore the sinogram was divided into ten regions for wedge thickness calculations, each corresponding to a single wedgelet. A wedglet is defined as all the rays passing through a single DBA wedge pair.[1] Wedge thicknesses are calculated using the method described in Szczykutowicz and Mistretta.[1] The wedge configurations are depicted in Fig. 2(c) and will be denoted by $H(i,v)$ where $i$ is wedgelet

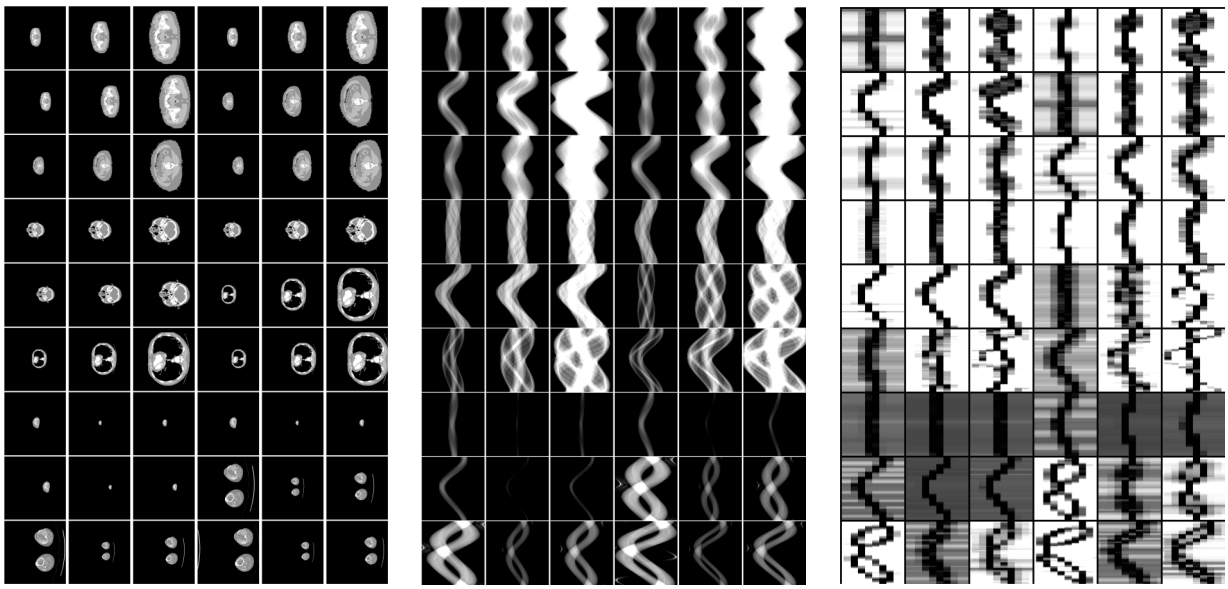

(a) (b) (c)

FIG. 2. (a) View of all of the digital phantoms used to construct the atlas set of wedge configurations. A head, shoulder, thorax, abdomen, wrist, and legs at three different sizes and at three different positions were studied. (b) Sinograms for each of the images shown in (a); horizontal axis is detector index, vertical axis is view angle for each of the sub images. (c) Wedge configurations (thicknesses) for each of the sinograms shown in (b); horizontal axis is wedge pair index, vertical axis is view angle for each of the sub images. In (c), as the shades of gray become darker, the represented wedge thickness decreases.

number and $v$ is an index ranging from 1 to *numConfigs*. The sinograms used to determine the wedge configurations in Fig. 2(c) are shown in Fig. 2(b). Any wedge pair thickness over 15 mm was set to 15 mm. The same desired level of detector signal was used in the wedge positioning algorithm for each body region/size/position combination. Milliampere modulation was simulated which allowed the number of photons incident onto the DBA wedge pairs to be set such that all configurations had at least one wedge pair of zero thickness. The zero thickness region corresponded to the most attenuating part of the projection. This explains why the wedge configuration sinograms shown in Fig. 2 for the smaller body regions require a smaller wedge thickness.

Atlas construction is an iterative process as observed in Fig. 3. It begins by computing the sum of the absolute differences in wedge pair thickness between all wedge configurations. A unique configuration occurs when the sum of the absolute difference computed between that configuration and all other configurations in the atlas is more than a threshold tr. In order to extract only the unique configuration from within $H(i,v)$, each configuration is compared to all other combinations as follows. The first configuration ($v = 1$) in $H(i,v)$ is added to the atlas library. Then, starting with the second ($v = 2$) configuration in $H(i,v)$, each configuration is compared with the other entries in the library. If the sum of the absolute difference between that configuration and all the configurations currently in the atlas is more than tr for all atlas library members, then that configuration is added to the atlas library. This process is repeated for all view angles ($v = 1$ to *numConfigs*) and produces a subset of DBA wedge configurations that span the space of all the configurations in $H(i,v)$, including all body regions, sizes, and positionings. During an actual DBA scan, the DBA would simply be restricted to atlas configurations for which the air-scan would be precalculated.

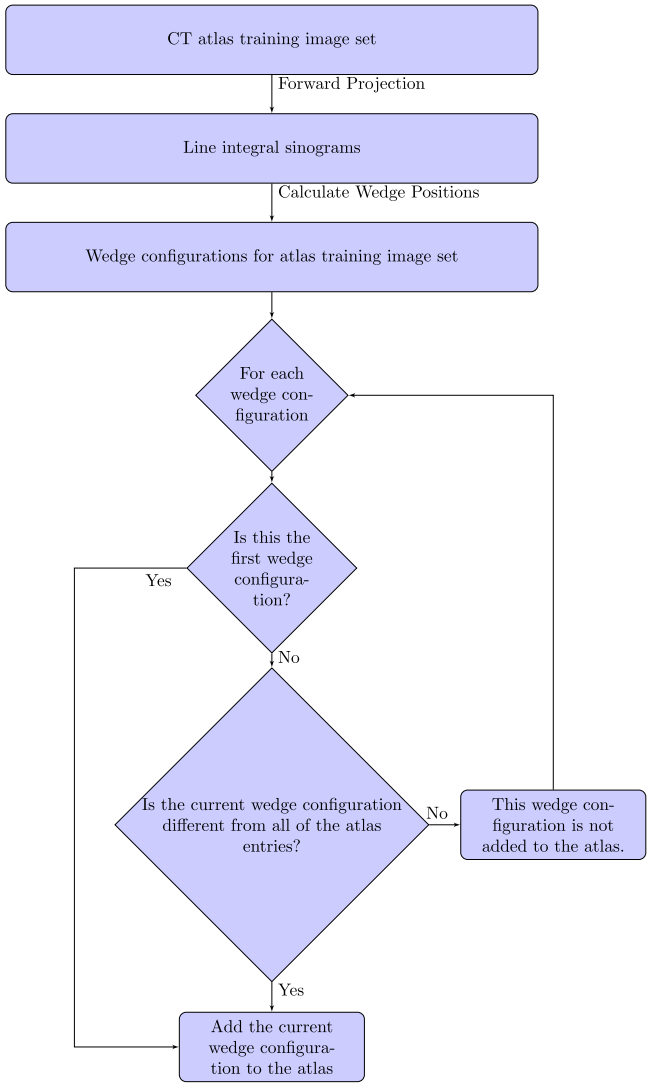


FIG. 3. Flowchart outlining the creation of an atlas of wedge configurations from a training set of CT images. See the text for more details.

## 2.B. Creation of the different body regions

Head, shoulder, thorax, abdominal, wrist, and leg anatomical CT axial slices were obtained from the (IMAIOS SAS image gallery, Montpellier, France). The images were converted to Hounsfield units using tissue attenuation values taken from NIST (Ref. 18) for cortical bone, soft tissue, and fat and a simple image based threshold for each of the materials. A monoenergetic 60 keV beam was simulated for the forward projection. These slices were then dilated using 2D linear interpolation to simulate different sizes and shifted to simulate patient off centering. The dilation amounts, as can be seen from Fig. 2(a), were tuned such that the slices occupied almost the entire 50 cm imaging field of view. At the smallest dilation amounts, the anatomy occupied roughly 1/3 of the field of view. Since 360° rotation scans were simulated, the rotation of the anatomy within the slices was not varied. The off centering amounts were 0, 3, and 8 cm. Dilation as performed here does not truly reflect the size differences between small and large patients. The internal bony structure of obese patients is quite similar to nonobese patients. Ideally, the test set of images used in the atlas creation process should reflect the patient population and procedure types for which the atlas based FFMCT is being used. We used the current set of images for convenience and suggest a custom image set for atlas generation be collected on an application driven basis.

## 2.C. Atlas construction for volume of interest DBA imaging

The number of wedge positions required for VOI imaging as implemented by our group previously [3,19] is actually given by the Gauss integer summation expression,

$$\text{No. of unique positions} = \frac{n\text{DBA}(n\text{DBA}+1)}{2}. \quad (1)$$

Equation (1) can be derived assuming only two positions are possible for each wedge; each wedge can either be set to its thickest or thinnest configuration. Also considering that only one VOI is imaged during an acquisition, for $n$DBA wedges, we can have $1, 2, \ldots, n$DBA wedges open (thinnest

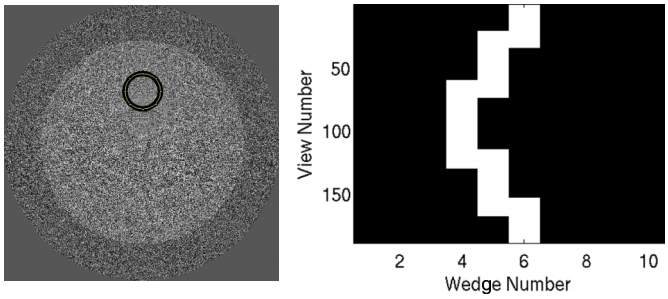


FIG. 4. (a) Location of the VOI. (b) Wedge position sinogram. In this binary sinogram, white and black represent wedges at minimum and maximum thicknesses, respectively. This wedge position sinogram allows an appreciation of how only 5 unique configurations are required.

position) and the rest of the wedge closed (thickest position) at a total of $n$DBA, $n$DBA$-1, \ldots, 1$ positions. Summing the total number of positions is simply the sum of integers 1 to $n$DBA. Assuming all of the possible DBA-VOI configurations are put into the atlas, there should be no difference in performance between using an atlas and not using an atlas for DBA-VOI imaging. More complicated VOI approaches would likely require a non binary wedge positioning scheme.[7]

An illustration of how only a small number of air-scans can be used for VOI imaging is apparent by analyzing Fig. 4. This figure depicts a DBA implemented VOI imaging acquisition in which a 2.5 cm VOI is identified within a uniform cylindrical phantom. It is easy to see in Fig. 4(b) that only five unique wedge configurations are required for this VOI. Therefore, instead of acquiring air-scan data at all of the view angles, only five view angles worth of air-scan data should have to be collected, corresponding to the five unique wedge configurations.

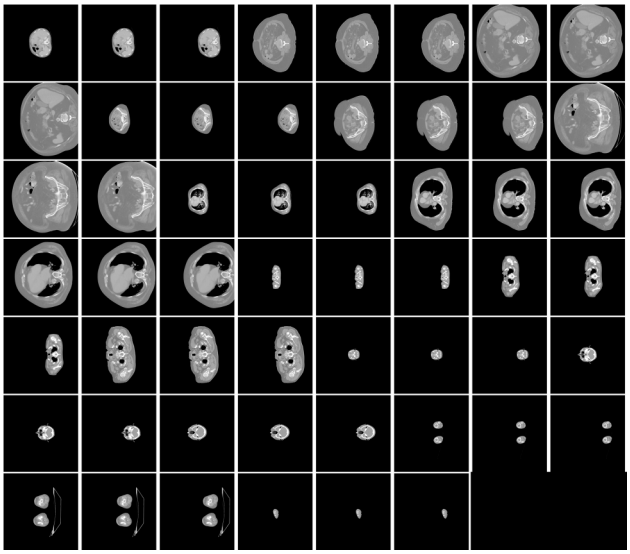

FIG. 5. Set of CT images used to evaluate the atlas methodology presented in this paper. These images are unique from the images shown in Fig. 2(a) and have no scaling applied, only varying amounts of off-centering.

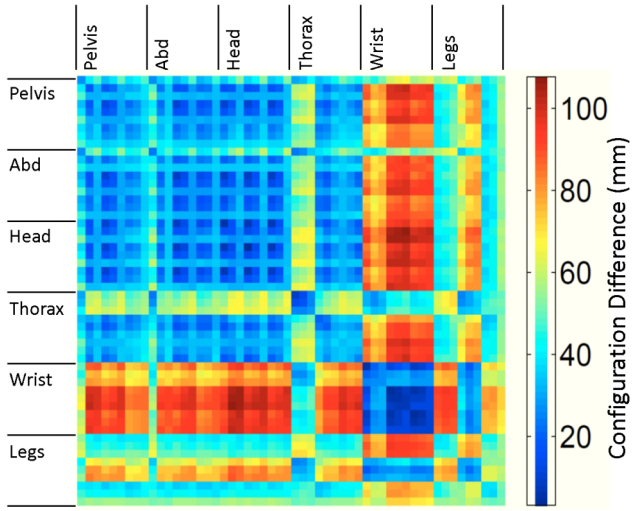


FIG. 6. Map of the mean absolute difference in wedge configuration between every wedge within $H(i,v)$. The values displayed are the mean over all of the view angles for a given body region/size/positioning amount configuration comparison. The structured nature of this map clearly demonstrates that some body regions, sizes, and position configurations require wedge positions very similar to other body region, size, and position combinations while other combinations require wedge configurations that differ greatly. Each grouping is ordered as follows: small centered, medium centered, large centered, small 3 cm offcentered, medium 3 cm offcentered, large 3 cm offcentered, small 8 cm offcentered, medium 8 cm offcentered, and large 8 cm offcentered.

### 2.D. Quantifying performance loss with atlas

To evaluate atlas performance, we obtained 18 axial slice CT scan images under IRB approval from our institution. The 18 images were of small, medium, and large sized abdomen, pelvis, thorax, shoulder, and head scans. Additionally, small and large images of the legs and a single sized wrist were

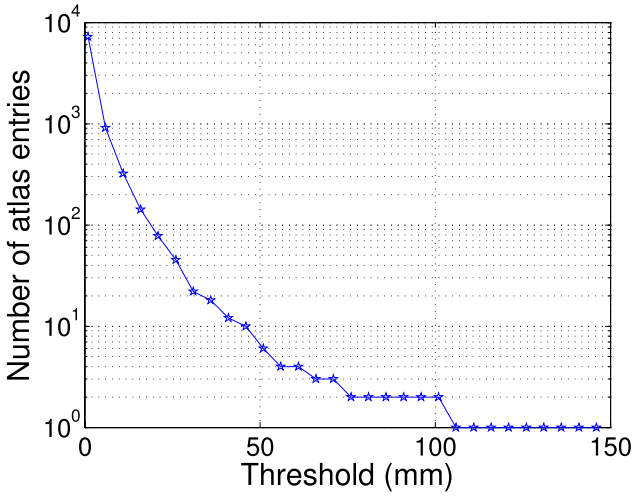


FIG. 7. Number of atlas entries as a function of threshold value. Here, the threshold value is the sum of the absolute difference between atlas entires. In other words, a very small threshold allows for atlas entries that are very similar to each other and therefore the total number of atlas entries required to span all the configurations shown in Fig. 2(c) is high relative to using a larger tr.

obtained. All 18 of the images were then off centered by 3 and 8 cm resulting in a total of 54 different clinical cases as shown in Fig. 5. The wedge pair thicknesses for each of these cases were calculated using the same method as images shown in Fig. 5.

The change in the number of photons incident on the body regions was computed with and without constraining the wedge configurations to an atlas. The number of photons incident to a patient was calculated assuming a 60 keV beam was attenuated by an iron wedge pair with a thickness equal to the profile defined by the wedge configuration. Due to the large number of body regions/size/position combinations studied, a histogram analysis was used to facilitate expressing the results of comparing the atlas approach to an unconstrained DBA-FFMCT scan. A plot of the ratio of the total number of photons incident with the atlas to the number incident with unconstrained imaging was made for each of the 54 clinical CT images. The number of photons was calculated using only those photons actually striking the body regions (i.e., those photons traversing only air were excluded from our analysis) and was summed for all view angles within a given body region/size/position. Additionally, a histogram was made which displays the total number of photons incident on the patient as a function of the number of atlas entries. This histogram represents the distribution of atlas photon count to unconstrained photon count for all of the body regions, sizes, and positions for a given tr value.

## 3. RESULTS AND DISCUSSION

### 3.A. Atlas creation

Figure 6 depicts the sum of the absolute difference for each of the wedge configurations shown in Fig. 2(c) computed with each other. The structured nature of this map clearly demonstrates that some body regions, sizes, and position configurations require wedge positions very similar to other body region, size, and position combinations. The figure also depicts regions showing large differences. One, for example, is the large difference in wedge pair design required for detector equalization when imaging a small wrist compared to a large abdomen. It is interesting to note the similarity between the smallest size thorax and the largest size wrist. The similarity is due to the heart and the wrist being of a similar size. Since the rest of the thorax does not produce attenuation of a magnitude similar to the heart, the heart dominates the positioning of the wedges and therefore requires a wedge configuration similar to the largest size wrist.

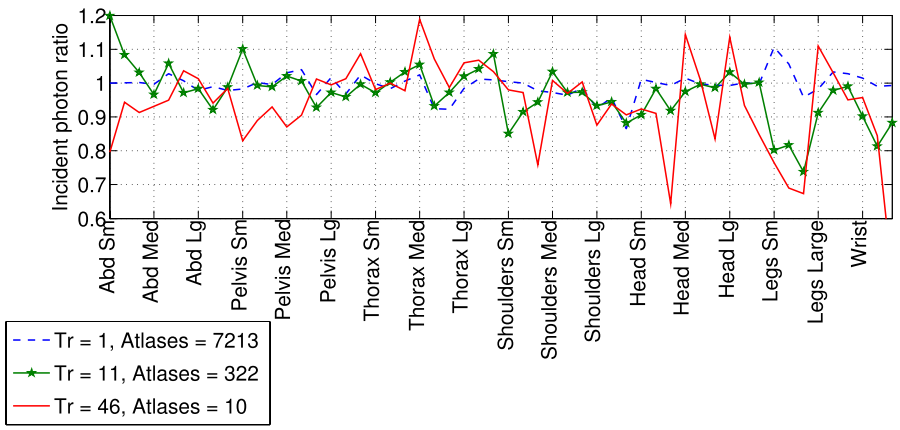


(a)

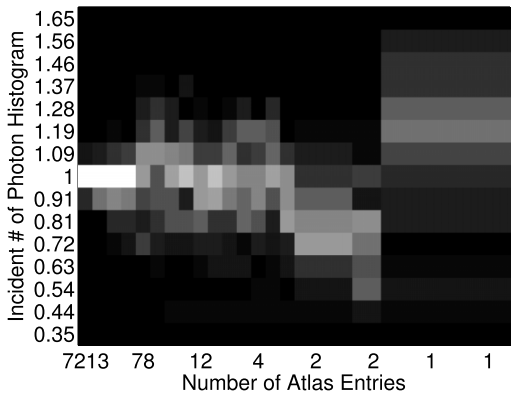


(b)

FIG. 8. (a) Plot of the number of photons incident on each phantom for the atlas case relative to the unconstrained case. In this figure, the abbreviations are as follows: Abd = Abdomen, Sm = Small, Med = Medium, and Lg = Large. Each case has three points corresponding to 0 cm: 0, 3, and 8 cm offcentering. (b) Graphical display of incident number of photon difference shown as a histograms as a function of atlas size. Here, the total number of photons incident on the patient histograms are made using all of the difference body region/size/off centering combinations for a given number of atlas configurations.

Using the algorithm described in Sec. 2.A, $H(i,v)$ can reduced to a much smaller subset of wedge configuration depending on the tr value chosen. Figure 7 depicts the number of atlas entries as a function of threshold number. As expected, as the threshold is increased the number of atlas entries decreases. This is due to our criteria for acceptance into the atlas which only allows new members if they are sufficiently different from members currently in the atlas as judged by the sum of the absolute difference.

### 3.B. Numerical results quantifying performance loss due to atlas

Figure 8(a) depicts the relative total number of photons incident on the patient between the atlas and unconstrained cases as a function of body region, size, and position for three different atlas entry numbers; 7213, 322, and 10. Figure 8(b) displays how quickly the histogram widens in terms of differences in the incident number of photons between the atlas and unconstrained cases as a function of atlas size. Assuming it is desired to keep the incident number of photons within ±20% of the unconstrained case, our results show that 322 atlas configurations would be required. The smaller of the two leg cases does deviate by slightly more than 20% from the unconstrained case. This is most likely due to the spacing difference between the legs in the atlas creation set of images and the leg image used to evaluate the atlas performance.

In a real world implementation of the atlas methodology for DBA-FFMCT and DBA-VOI imaging, the total number of atlas configurations required to be measured would be the number required for DBA-FFMCT plus the number for VOI imaging. In this case, using our ±20% of the incident number of photons criteria, this would correspond to 322 plus 55 wedge positions required for air-scan measurement. As to how many different kV stations these air-scan measurements would need to be acquired at, further work would be needed and this would likely be a function of the detector and tube/generator of a specific CT or CBCT system.

It should also be noted that we inherently assume the DBA would be capable of being positioned to an air-scan precalibrated position within the inter pulse delay of a CBCT system. For diagnostic CT in which the tube is always on and individual view angles are averaged over view angle, the methodology presented in this paper would need to be altered to account for wedges being in positions that were not calibrated. On CBCT systems that allow for view angles to be acquired in a pulsed mode, the DBA could be positioned while the x-ray tube is off to a precalibrated position; this could not be done for a CT system in which projection data are continuously collected.

For systems with kV modulation, the atlas would have to be measured at each allowable kV station or at a few stations and an interpolation/extrapolation scheme used to cover the rest of the allowable kV stations. Additionally, generator stability issues may require the atlas to be altered before being used to log normalize projection data. This type of data correction is well known to manufacturers and is usually proprietary in its implementation.

## 4. CONCLUSIONS

This work outlines a clinically feasible solution for the determination of air-scan free DBA-FFMCT imaging. In addition, the methodology presented here could also be applicable to the FFMCT technology implemented by other research groups such as Hsieh and Pelc[4,5] or the simulation work being carried out by Bartolac and Jaffray.[6–8] In addition, the technique described in this work should have applications in volume of interest imaging (VOI).[9–13] All of these techniques rely on imaging with a fluence field that changes from view to view or changes on a patient to patient basis.

Researchers working in FFMCT wishing to apply this methodology would likely have differing reasons as to why they are implementing FFMCT. FFMCT allows for regionally varying noise prescriptions, detector dynamic range reductions, dose reductions, and a reduction in scatter to primary ratio. Each of these advantages would likely require a unique metric for determining the number of atlas positions. We chose the relative number of photons striking the imaging object here to illustrate one possible metric. This method does not ensure one obtains the minimum number of configurations required to match the performance of an unconstrained modulator. This method only ensures the atlas contains unique entries as determined by the choice of the threshold value. Since we determine the threshold based on a plot of the performance metric versus the threshold, it can be safely inferred that this method will provide an atlas of near optimal size. As mentioned in Sec. 3.B, work remains in adapting this technique for systems which do not pulse the x-ray beam which therefore limits this methodology to pulsed CT systems.

## ACKNOWLEDGMENT

This work is supported by a grant from Siemens Medical Systems (AX division Hoffman Estates, IL).

[a]Author to whom correspondence should be addressed. Electronic mail: TSzczykutowicz@uwhealth.org

[1]T. Szczykutowicz and C. Mistretta, "Design of a digital beam attenuation system for computed tomography: Part i. System design and simulation framework," Med. Phys. **40**, 021905 (12pp.) (2013).
[2]T. Szczykutowicz and C. Mistretta, "Design of a digital beam attenuation system for computed tomography: Part ii. Performance study and initial results," Med. Phys. **40**, 021906 (9pp.) (2013).
[3]T. Szczykutowicz and C. A. Mistretta, "Experimental realization of fluence field modulated ct using digital beam attenuation," Phys. Med. Biol. **59**, 1305–1326 (2014).
[4]S. S. Hsieh and N. J. Pelc, "The feasibility of a piecewise-linear dynamic bowtie filter," Med. Phys. **40**, 031910 (12pp.) (2013).
[5]S. S. Hsieh and N. J. Pelc, "Optimized control of a dynamic, prepatient attenuator," Proc. SPIE **8668**, 86681Q (2013).
[6]S. Bartolac, S. Graham, J. Siewerdsen, and D. Jaffray, "Compensator approaches for intensity modulated computed tomography," in *International Conference on Image Formation in X-ray Computed Tomography* (University of Utah, Salt Lake City, UT, 2010), Vol. 1, p. 101.
[7]S. Bartolac, S. Graham, J. Siewerdsen, and D. Jaffray, "Fluence field optimization for noise and dose objectives in ct," Med. Phys. **38**, S2–S17 (2011).
[8]S. Bartolac and D. Jaffray, "Fluence field modulated computed tomography," in *International Conference on Image Formation in X-ray Computed Tomography* (University of Utah, Salt Lake City, UT, 2012), Vol. 2, pp. 119–122.

[9]D. Kolditz, Y. Kyriakou, and W. Kalender, "Volume-of-interest (voi) imaging in c-arm flat-detector ct for high image quality at reduced dose," Med. Phys. **37**, 2719–2730 (2010).
[10]D. Heuscher and F. Noo, "Ct dose reduction using dynamic collimation," in *IEEE Nuclear Science Symposium and Medical Imaging Conference (NSS/MIC)* (IEEE, Valencia, Spain, 2011), pp. 3470–3473.
[11]D. Heuscher and F. No, "Ct dose reduction using dynamic collimation," in *The Second International Conference on Image Formation in X-Ray Computed Tomography* (University of Utah, Salt Lake City, UT, 2012), pp. 115–118.
[12]L. Chen, L. Yu, S. Leng, and C. McCollough, "Ct volume-of-interest (voi) scanning: Determination of radiation reduction outside the voi," RSNA **SSK15-07** (2011).
[13]M. Oktay and F. Noo, "Reduction of dose by focusin the x-ray beam to a specific region of interest: Monte Carlo assessment," in *The Third International Conference on Image Formation in X-Ray Computed Tomography* (University of Utah, Salt Lake City, UT, 2014), pp. 279–282.
[14]T. Szczykutowicz and J. R. Hermus, "Fluence field modulated CT on a clinical TomoTherapy radiation therapy machine," Proc. SPIE **9412** (2015) (to be published).
[15]T. Szczykutowicz and J. Hermus, "Fluid dynamic bowtie attenuators," Proc. SPIE **9412** (2015) (to be published).
[16]P. Shunhavanich, S. Hsieh, and N. J. Pelc, "Fluid-filled dynamic bowtie filter: A feasibility study," Proc. SPIE **9412** (2015) (to be published).
[17]S. S. Hsieh and N. J. Pelc, "The piecewise-linear dynamic attenuator reduces the impact of count rate loss with photon-counting detectors," Phys. Med. Biol. **59**(11), 2829–2847 (2014).
[18]J. Hubbell and S. Seltzer, "Tables of x-ray mass attenuation coefficients and mass energy-absorption coefficients 1 keV to 20 MeV for elements Z = 1 to 92 and 48 additional substances of dosimetric interest," No. PB–95-220539/XAB; NISTIR–5632. National Inst. of Standards and Technology-PL, Gaithersburg, MD. Ionizing Radiation Div., 1995.
[19]T. Szczykutowicz and C. Mistretta, "Volume of interest ct implemented with a dynamic bowtie filter," Proc. SPIE **8313**, 86682R (2013).